
WORKING MEMORY GRAPHS

Ricky Loynd, Roland Fernandez, Asli Celikyilmaz, Adith Swaminathan & Matthew Hausknecht

Microsoft Research AI

{riloynd, rfernand, aslicel, adswamin, mahauskn}@microsoft.com

ABSTRACT

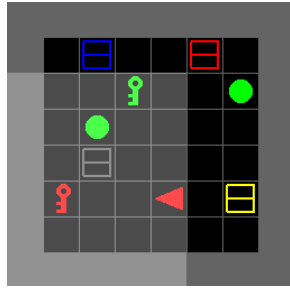
Transformers have increasingly outperformed gated RNNs in obtaining new state-of-the-art results on supervised tasks involving text sequences. Inspired by this trend, we study the question of how Transformer-based models can improve the performance of sequential decision-making agents. We present the Working Memory Graph (WMG), an agent that employs multi-head self-attention to reason over a dynamic set of vectors representing observed and recurrent state. We evaluate WMG in two partially observable environments, one that requires complex reasoning over past observations, and another that features factored observations. We find that WMG significantly outperforms gated RNNs on these tasks, supporting the hypothesis that WMG’s inductive bias in favor of learning and leveraging factored representations can dramatically boost sample efficiency in environments featuring such structure.

1 INTRODUCTION

Because of their ability to process sequences of data, gated Recurrent Neural Networks (RNNs) have been widely applied to natural language processing (NLP) tasks such as machine translation. In the RNN-based approach of Sutskever et al. (2014), an encoder RNN maps an input sentence to a series of internal hidden state vectors. The encoder’s final hidden state is copied into a decoder RNN, which then generates another sequence of hidden states that determine the selection of output tokens in the target language. This model can be trained to translate sentences, but translation quality deteriorates on long sentences where long-term dependencies become critical. Reasoning that this drop in performance is due to the limited representational capacity of an RNN’s hidden state vector, Bahdanau et al. (2014) boosted translation quality by applying an attention mechanism to create paths serving as shortcuts from the input to the output sequences, routing information outside the linear chain of the RNN’s hidden states. Similar attention mechanisms have since gained wide usage, culminating in the Transformer model (Vaswani et al., 2017) which replaces the RNN with many short paths of self-attention. Since then, Transformers have outperformed RNNs on many NLP tasks (Devlin et al., 2018).

We seek to leverage these intuitions to improve the ability of Reinforcement Learning (RL) agents to reason over long time horizons in Partially Observable Markov Decision Processes (POMDPs) (Kaelbling et al., 1998). In a POMDP, a single observation Obs_t is not sufficient to identify the latent environment state s_t . Thus the agent must reason over the history of past observations in order to select the best action for the current step. A simple strategy employed by DQN (Mnih et al., 2015) is to condition the policy on the N most recent observations $\pi(a_t|Obs_{t-N} \dots Obs_t)$. But in complex environments, the sufficient number N may be large, highly variable, and unknown. To address this issue, gated RNNs such as LSTMs (Hochreiter & Schmidhuber, 1997) and GRUs (Chung et al., 2015) use internal, recurrent state vectors which in theory can maintain information from past observations (Hausknecht & Stone, 2015; Oh et al., 2016). However, in practice, these methods are limited by the single path of information flow defined by the linear chain of RNN hidden states. As in NLP, we hypothesize that providing alternative paths for information will be advantageous to RL agents. Building on this intuition, we introduce the Working Memory Graph (WMG), a Transformer-based agent that uses self-attention to provide a multitude of shortcut paths for information to flow between the past observations and the current action.

In addition to providing many paths for information, Transformers are also well suited for handling variably-sized inputs such as words in a sentence. Although most Reinforcement Learning environ-



Instruction: *Pick up the green key*

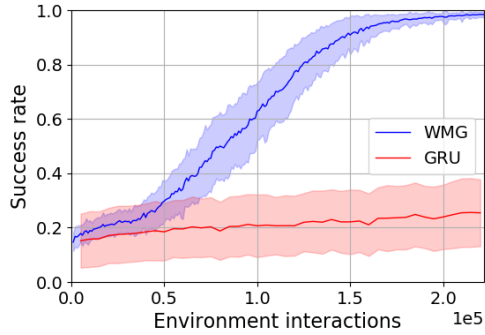


Figure 1: **Left:** BabyAI rewards the agent (red triangle) for performing the task given by the instruction. **Right:** Our Transformer-based model (WMG) leverages factored observations and shortcut recurrence to solve this partially observable BabyAI task (PickupLoc) in far fewer environment interactions than a GRU-based agent using the same factored observations.

ments provide fixed-sized feature spaces, certain environments have observations spaces amenable to factorization. As a motivating example, consider the BabyAI environment (Chevalier-Boisvert et al., 2018) depicted in Figure 1 (left). The native observation space is the agent’s field of view, a 7x7 grid, shown in lighter grey. This observation can be efficiently represented by a set of factors describing the types, colors, and relative x and y coordinates of all visible objects:

$$([\text{green, key, 1, 3}], [\text{grey, box, 2, 1}], [\text{green, ball, 2, 2}], [\text{red, key, 3, 0}])$$

This *factored observation* is more compact than the native observation, but will vary in size depending on the number of objects in view. Motivated by prior work on factored representations (Russell & Norvig, 2009) and factored MDPs (Boutillier et al., 2000; 2001), we explore the idea of encoding factored observations as input to Transformer-based agents. In particular, we compare how factored observations affect the learning speed of Transformer and RNN-based agents.

Our contributions are twofold: First we introduce the *Working Memory Graph* (WMG), a Transformer-based agent implementing a novel form of *shortcut recurrence* which we demonstrate to be effective at complex reasoning over long-term dependencies. Second, we identify the synergy between Transformer-based RL architectures and *factored observations*, demonstrating that by virtue of its Transformer-style self-attention, WMG is able to effectively leverage factored observations to learn high-performing policies given an order of magnitude fewer environment interactions than alternative architectures. To preview our findings, Figure 1 (right) shows an example of the dramatic boosts in sample efficiency obtained through the combination of shortcut recurrence and Transformer-based processing of factored observations.

2 WORKING MEMORY GRAPH

Broadly, WMG incorporates an inductive bias in favor of learning and leveraging factored representations, including both observed and unobserved (latent) factors. Observed factors are represented by multiple input vectors called *percepts*. Latent factors are represented by multiple recurrent vectors called *concepts*. Instead of handling long-range dependencies over time by applying self-attention to a long history of observations, for which the quadratic computational cost could be prohibitively expensive, WMG relies on its much more limited set of concepts to represent long-range dependencies. The term *Working Memory Graph* is motivated by the relatively *limited* size of WMG’s self-attention computation graph, in loose analogy with the cognitive science term *working memory*, which refers to a cognitive system that holds a limited amount of information for use in mental processing. (Miller, 1956)

WMG introduces *shortcut recurrence*, which replaces a gated RNN’s single path of information flow with a network of shorter self-attention paths. As illustrated in Figure 2 (right), WMG’s shortcut

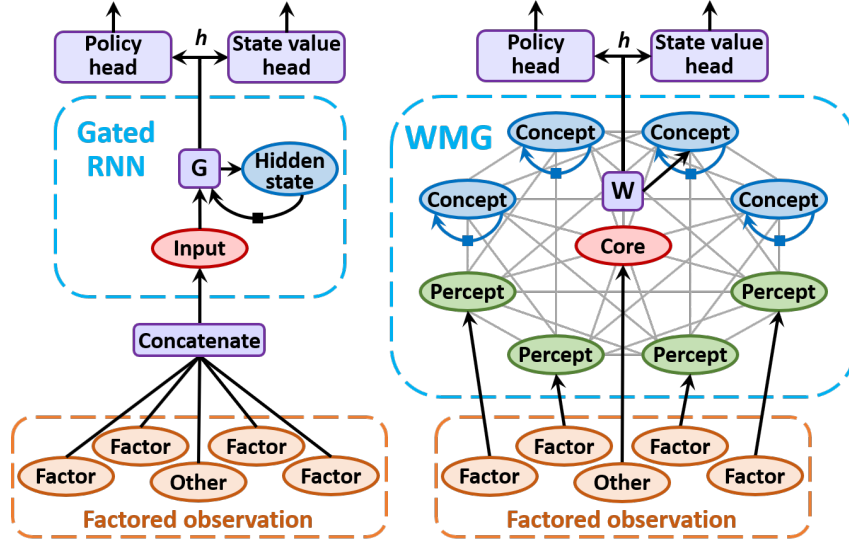


Figure 2: Schematic diagrams of two RL agent architectures taking input from a factored observation. **Left:** A gated RNN constrains information to flow through a linear path of fixed-length vectors. (G denotes the internal vector operations of a GRU or LSTM.) **Right:** WMG allows information to flow through many self-attention paths among a network of vectors. (W denotes WMG’s embedding and multi-layer Transformer operations.) WMG replaces the RNN’s recurrent hidden state with a recurrent network of concept vectors, and replaces the RNN’s single observation input vector with a network of vectors including percepts mapped to observation factors.

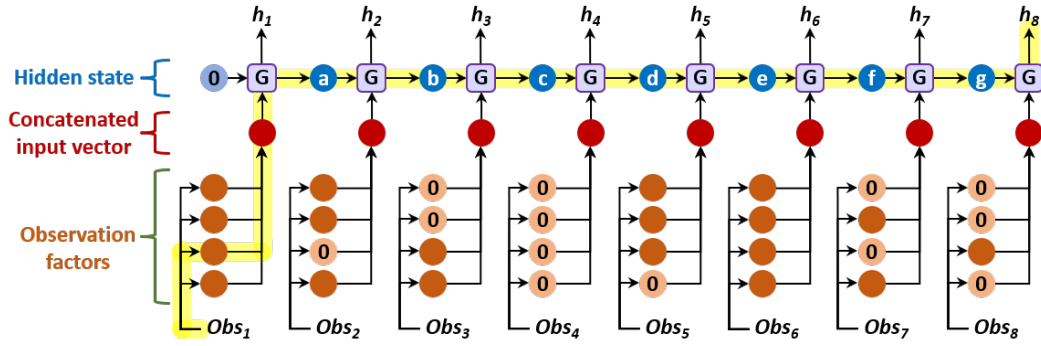
recurrence applies multi-head self-attention to a dynamic set of hidden state vectors, the aforementioned concepts, to simultaneously represent multiple latent factors or aspects of partially observable environments. Formally, each concept vector defines one row in a concept matrix $C \in \mathbb{R}^{n_C \times d_C}$, where n_C is the number of concepts maintained by WMG and d_C is the dimension of each concept vector. On each time step, the oldest concept is replaced by a new one.

WMG applies self-attention to observations by introducing multiple observation input vectors, percepts, as depicted in Figure 2 (right). In our experiments, a single percept encodes either an entire observation from a window of recent observations, or one factor (such as a green key in BabyAI) of a factored observation. On each time step, WMG receives a formatted observation consisting of a variable number of (n_P) percept vectors forming a percept matrix $P \in \mathbb{R}^{n_P \times d_P}$, and a core vector $c \in \mathbb{R}^{d_c}$ that contains any other observation information (such as any non-factored portions of the current observation). The core, percept and concept vectors are stacked into one matrix for input to WMG’s Transformer operation:

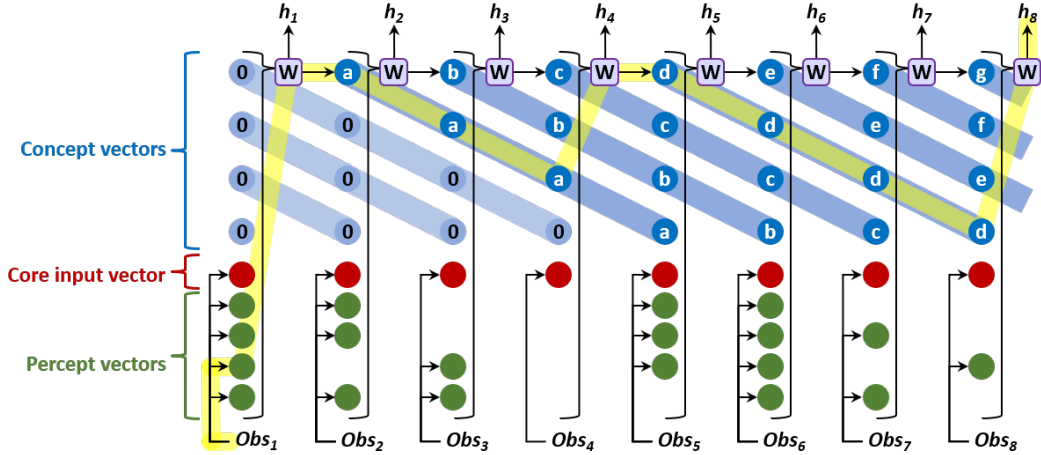
$$T^{in} = \begin{bmatrix} cW_{core} + b_{core} \\ PW_{per} + b_{per} \\ C'W_{con} + b_{con} \end{bmatrix}, \quad C' = [C \ I]$$

where $W_{core} \in \mathbb{R}^{d_c \times d_T}$, $W_{per} \in \mathbb{R}^{d_P \times d_T}$ and $W_{con} \in \mathbb{R}^{(d_C + n_C) \times d_T}$ are embedding matrices with corresponding bias vectors $b \in \mathbb{R}^{d_T}$ broadcast over rows, and each concept is concatenated with a one-hot age vector. Closely following the encoder architecture of Vaswani et al. (2017), WMG’s Transformer operation takes the input matrix $T^{in} \in \mathbb{R}^{n_T \times d_T}$ and returns an output matrix $T^{out} \in \mathbb{R}^{n_T \times d_T}$, where $n_T = 1 + n_P + n_C$ is the number of input (or output) nodes, and d_T is the size of each node vector. The oldest concept is replaced by a new concept vector generated as a non-linear function of the core node’s output vector $h = T_{1,:}^{out}$:

$$C = \begin{bmatrix} \tanh(hW_C + b_C) \\ C_{-n_C,:} \end{bmatrix}, \quad W_C \in \mathbb{R}^{d_T \times d_C}, \quad b_C \in \mathbb{R}^{d_C}$$



(a) Gated RNN unrolled in time.



(b) WMG unrolled in time.

Figure 3: **Shortcut Recurrence:** In a Gated RNN, for the first observation Obs_1 to affect the agent’s output h_8 , information must pass through 8 gating operations and 7 intervening hidden states $\mathbf{a-g}$. In contrast, in a WMG, many possible paths lead from the first observation to the output h_8 . The highlighted path requires only three passes through \mathbf{W} , and is stored unchanged for several time steps in concept vectors \mathbf{a} and \mathbf{d} . This example illustrates how WMG’s concept nodes provide shorter paths for information to flow forward and gradients to flow backward.

The trainable parameters θ of WMG and its Transformer layers are trained end-to-end through back-propagation of a policy-gradient loss maximizing the cumulative expected return $\mathcal{J}(\theta)$:

$$\nabla_{\theta} \mathcal{J}(\theta) = \mathbb{E}_{\pi} \left[\sum_{t=0}^{\infty} \nabla_{\theta} \log \pi(a_t | \mathbf{h}_t; \theta) A^{\pi}(Obs_t, a_t) + \beta \nabla_{\theta} H(\pi(\mathbf{h}_t; \theta)) \right]$$

where $\pi(a | \mathbf{h}_t; \theta)$ denotes WMG’s policy head operating on hidden state \mathbf{h}_t , H is the entropy of the policy’s action distribution, and β controls the strength of the entropy regularization term. To reduce the variance of gradient estimates, we use the advantage actor-critic algorithm described by Mnih et al. (2016), which estimates the advantage $A^{\pi}(s_t, a_t)$ using a γ -discounted k -step return as follows:

$$A^{\pi}(Obs_t, a_t) = \left(\sum_{i=0}^{k-1} \gamma^i r_{t+i} \right) + \gamma^k V^{\pi}(\mathbf{h}_{t+k}) - V^{\pi}(\mathbf{h}_t; \theta)$$

where $V(\mathbf{h}_t; \theta)$ denotes WMG’s state-value head, which is trained to minimize the squared difference between the k -step return and the current value estimate: $\|(\sum_{i=0}^{k-1} \gamma^i r_{t+i} + \gamma^k V^{\pi}(\mathbf{h}_{t+k})) - V(\mathbf{h}_t)\|_2^2$, and k is upper-bounded by the number of time steps (t_{max}) in the actor’s current update window.

To summarize WMG’s operation, Figure 3 compares the flow of information through a gated RNN and through WMG, illustrating how WMG’s concept vectors latch information unchanged for multiple time steps to create shorter paths for information flow in both the forward and backward passes.

3 RELATED APPROACHES

Having explained how WMG operates, we distinguish it from related work: Prior approaches have used attention for memory access (Graves et al., 2016; Oh et al., 2016) or self-attention to process individual observations (Zambaldi et al., 2019; Vinyals et al., 2019). These approaches all used LSTM-based recurrence over time. In contrast, WMG obviates the need for gated recurrence by applying self-attention to a network of concept vectors which are persisted through time.

Other Transformer-based models handle partial observability using state vectors analogous to WMG’s concepts, but with different state-update schedules: RMC (Santoro et al., 2018) updates all state vectors on every time step, while RIMs (Goyal et al., 2019) enforces sparsity by updating exactly half of the state vectors (called *RIMs*) on each step. WMG replaces only one concept on each time step in order to maximize the persistence of latched concept vectors and thereby extend the reach of the shortcut paths that they create from inputs to outputs. And unlike WMG, RMC and RIMs use gated RNNs to update their state vectors.

Unlike the other models discussed here, the Gated Transformer-XL (Anonymous, 2019) addresses partial observability by feeding hundreds of past observations at once into the Transformer. By contrast, in order to mitigate the $O(N^2)$ computational cost of self-attention, WMG computes self-attention over a comparatively small number of concepts which capture and maintain the relevant aspects of past observations.

4 EXPERIMENTS

In our experiments, we aim to (1) evaluate WMG’s ability to reason over long time spans in a setting of high partial observability, and (2) understand how factored representations may be effectively utilized by WMG. To address these questions we present results on two environments: a novel Pathfinding task which requires complex reasoning over past observations, and the BabyAI domain (Chevalier-Boisvert et al., 2018) which involves changing goals, partial observability, and observations that can be readily factored. To foreshadow our results, the Pathfinding task demonstrates the effectiveness of WMG’s shortcut recurrence, and BabyAI demonstrates that WMG leverages factored observations to deliver very large gains in sample efficiency.

4.1 PATHFINDING TASK

The Pathfinding task is designed to evaluate WMG’s ability to perform complex reasoning over past observations. Figure 4 depicts the incremental construction of a directed graph over nodes identified by unique pattern vectors which are randomly generated on every episode. (See Appendix A for the graph-construction algorithm and other details.) On odd time steps the agent observes two pattern nodes to be linked, and on even steps the agent must indicate whether or not a directed path exists from one given pattern to another. As this cycle repeats, the graph grows larger and the agent must perform an increasing number of reasoning steps to confirm or deny the existence of a path between arbitrary nodes. Because the observation only contains incremental information and the entirety of the graph is never directly observed, the agent must leverage information from previous observations to infer connectivity between nodes.

For example, consider step 4 of Figure 4: To determine whether a path exists from green to yellow, the agent must recall and combine information from steps 1 and 3. Similarly, on step 12, if the agent were asked about the existence of a path from cyan to yellow, answering correctly without guessing would require piecing together information from three non-contiguous time steps. Since the actual quiz on step 12 asks whether a path exists from green to blue, the agent must reason over many past observations to determine that no such path exists.

Each pattern is a vector of D real numbers drawn randomly from the interval -1 to 1 . A binary value is added to the observation vector to indicate whether the current step is a quiz step, bringing

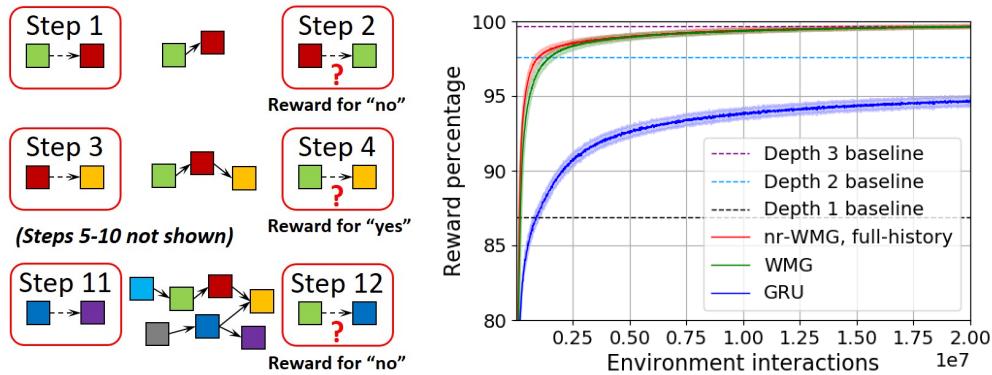


Figure 4: **Left: One episode of the Pathfinding task**, in this work, consists of 12 time steps with a maximum graph size $N = 7$ patterns. The boxes with rounded corners illustrate the observations for the given time steps, where a question mark identifies the step as a quiz step rather than a construction step. The box colors represent distinct pattern vectors. **Right: Results on Pathfinding:** Each plotted point is the percentage of reward on quiz steps received by the agent over the previous 10k time steps, averaged over 100 independent training runs. Bands display one standard deviation. (See Table 9 for more details.)

the size of the observation space to $2D + 1$, where $D = 7$ for our experiments. The action space consists of two actions, defined as *yes* or *no*. If the agent answers correctly on a quiz step, it receives a reward of 1; otherwise, it receives a reward of 0. The quiz questions are constructed to guarantee that each answer (*yes* or *no*) is correct half the time, so agents that act randomly or have no memory will obtain 50% of possible reward in expectation.

WMG is configured with concept nodes to handle the partial observability but no percept nodes, since we are not using this task to explore factored observations. The number of concept nodes is a tuned hyperparameter, equal to 16 in this experiment. (See Table B for all settings.) Each observation is passed directly to WMG’s core node, and WMG generates a new concept on each time step. We compare WMG’s performance to several baselines. Each *Depth- n* baseline is a hand-coded algorithm demonstrating the performance obtained using perfect memory of past observations and reasoning over paths up to n steps long. For example, *Depth-2* remembers all previous construction steps, and reasons over all paths of depth 2. Finally, in order to understand the effectiveness of concept nodes at capturing past information, we evaluate a *full-history*, non-recurrent version of WMG by removing the concept nodes and giving it all past observations on each time step, each one passed to a separate percept node.

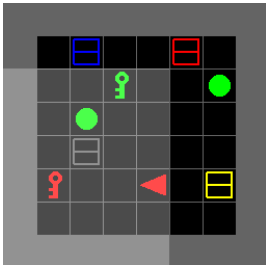
As shown in Figure 4, the GRU-based agent exceeds *Depth-1* performance, but remains well short of *Depth-2* performance after 20 million steps of training (environment interactions). In contrast, both versions of the WMG agent nearly reach *Depth-3* performance, demonstrating a greater ability to perform complex reasoning over past observations. The best performance is achieved by the nr-WMG with full-history, which has no need for recurrence. But the full WMG (with concepts) is nearly as sample efficient as this perfect-memory baseline. These results indicate that shortcut recurrence enables WMG to learn to store and utilize essential information from past Pathfinding observations in a more effective manner than a GRU.

4.2 BABYAI ENVIRONMENT

In order to understand how factored representations may be effectively utilized by WMG, we study BabyAI, a domain whose observation space is amenable to factorization. BabyAI (Chevalier-Boisvert et al., 2018) is a partially observable, 2D grid-world containing objects that can be viewed and moved by the agent. Unlike most RL environments, BabyAI features text instructions that specify the goal the agent needs to achieve, such as “pick up the green box.”

We focus on five BabyAI levels, for which the environment consists of a single 6x6 room, as shown in Figure 5 (left). Despite the apparent simplicity of a single-room domain, learning to solve it

can often take model-free RL agents hundreds of thousands of environment interaction steps. The agent’s action space consists of 7 discrete actions: Move forward, Turn left, Turn Right, Pick up, Drop, Toggle, and Done. An episode ends after 64 time steps, or when the agent achieves the goal, for which it receives a reward of 1. In Level 1 (GoToObj), the room contains only one object. The agent completes the mission by moving to an adjacent square and pointing toward the object. In Level 2, the target object is always a red ball, and seven grey boxes are present as distractors. In Level 3, the distractors may be any of the 3 object types and 6 colors. If one of the distractors happens to be a red ball, the agent is rewarded for reaching it. In Level 4, the instruction specifies the color and type of the target object. This is the first level in which the text instruction contains valuable information. (See Table 12 for instruction templates.) Level 5 increases the difficulty of Level 4 in two ways. First, the agent must not only reach the target object, but must also pick it up. Second, if multiple qualifying target objects are present, the agent is given the initial relative location of the true target, such as “behind you”.



Part of observation	Variable assignments	Node
Factored image	color= green , type= key , X=3, Y=1	percept
Factored image	color= grey , type= box , X=1, Y=2	percept
Factored image	color= green , type= ball , X=2, Y=2	percept
Factored image	color= red , type= key , X=0, Y=3	percept
Factored image	vertical wall X=-2	core
Factored image	horizontal wall Y=4	core
Factored instruction	command= go to , article= the , color= yellow , type= box , loc= None	core
Additional info	orientation= west , last action= move forward	core

Instruction:
Go to the yellow box

Figure 5: One completely factored observation, where each variable assignment corresponds to a one-hot vector in the full observation vector. Since the number of objects in an observation can vary, each object’s vectors are concatenated then passed to a percept node. All other one-hot vectors from the observation are concatenated then passed to the core node. X & Y coordinates refer to a frame of reference with the agent at the origin, pointed in the positive Y direction. The agent always observes one vertical wall and one horizontal wall.

Each agent observation in BabyAI consists of a text instruction, an image, and the agent’s orientation. The image’s native format is a 7x7 array of cell descriptors (not pixels) identifying three attributes of each cell: type, color, and open/closed/locked (referring to doors, which are not found in these 5 levels). To study factored observations in BabyAI, we define a factored representation, depicted in Figure 5. In our experiments the text instruction is always factored, but the image is formatted in multiple ways: (1) **7x7x3**, the native BabyAI image array; (2) **flat**, the native 7x7x3 array flattened to one vector; (3) **factored** image, as described in Figure 5. (*Note* that when a factored image is passed to a GRU, it must first be flattened and padded to form a fixed-length vector.)

To determine whether WMG can leverage factored observations more effectively than gated RNNs in BabyAI, we evaluate the following agents: (1) **WMG** is the full, recurrent WMG model, with percepts mapped to observation factors, (2) **nr-WMG** is an ablated, non-recurrent version of WMG with no concepts, (3) **GRU** is a GRU model, and (4) **CNN+GRU** uses a CNN to process the native 7x7x3 image, followed by a GRU. This CNN is one of the two CNN models provided in the BabyAI open source code (Chevalier-Boisvert et al., 2018).

4.2.1 RESULTS

Factored Observations: The largest performance differences in Table 1 stem from the choice of factored versus flat or native image formats. Notably, WMG with factored images can achieve sample efficiencies 10x greater (on Level 3) than CNN+GRU using the native 7x7 image format. However, factored observations alone are not sufficient for sample efficiency: WMG utilizes factored images much more effectively than a GRU on Levels 2-5. This result supports our hypothesis that Transformer-based models are particularly well suited for operating on set-based inputs like factored observations, and large gains in sample efficiency are observed as a result.

Table 1: **BabyAI sample efficiency**: the amount of training (shown here in thousands of environment interactions) required for a model to solve 99% of 10,000 episodes. Hyperparameters were first tuned on each model/format/level combination separately, then each reported result was computed as the median sample efficiency over 100 additional training runs. Dashes indicate that no model reliably reached a solution rate of 99% within 6 million training steps (environment interactions). Note that Chevalier-Boisvert et al. (2018) report sample efficiencies in terms of episodes rather than environment interactions. (See Table 12.)

Model Image format	WMG factored	nr-WMG factored	GRU factored	WMG flat	GRU flat	CNN+GRU native 7x7x3
1 - GoToObj	1.6	1.4	1.7	15.0	19.0	10.6
2 - GoToRedBallGrey	6.7	5.2	24.6	29.0	31.0	22.3
3 - GoToRedBall	16.0	23.6	174.4	92.0	124.6	204.9
4 - GoToLocal	59.7	71.3	2,241.6	1,379.9	1,799.4	—
5 - PickupLoc	222.3	253.0	—	—	—	—

Concept Nodes: Without factored observations, WMG-flat slightly outperforms GRU-flat, suggesting that shortcut recurrence implemented by the WMG’s concept nodes compares favorably to the GRU’s gated recurrence. With the benefit of factored observations, the non-recurrent ablation of WMG (nr-WMG) performs slightly better than the full WMG on the simplest two levels. But for the more challenging levels 3-5, WMG’s concept vectors prove to be of benefit for WMG with factored observations.

Early vs Late instruction fusion: Interestingly, within our training limit of 6 million environment interactions, CNN+GRU is unable to learn to solve the levels (4 & 5) where instructions carry important information. We suspect this is because the CNN processes just the image while the factored instruction is passed directly to the GRU, skipping the CNN. By contrast, the baseline BabyAI agent uses FiLM layers to integrate the processing of the image with the text instruction. Both WMG and GRU models can process the image and instruction together in all levels of processing. This early fusion appears to allow all WMG and GRU models to solve Level 4.

In summary, the two WMG models with factored images were the only agents able to solve Level 5, and they learned to do so in approximately the same number of interactions that CNN-GRU required to solve Level 3. These drastic differences in sample efficiency serve to highlight the potential gains that can be achieved by RL agents equipped to utilize factored observations.

While WMG’s sample efficiencies dramatically exceed the RL benchmarks published with the BabyAI domain (Chevalier-Boisvert et al., 2018), often by two orders of magnitude (Table 12), it’s important to note that these sets of results are not directly comparable. Our experiments all used factored text instructions, and each model’s hyperparameters were tuned for each level separately, while the BabyAI benchmark agent was trained on all levels using the single hyperparameter configuration provided in the BabyAI release. Because of these differences, our experiments should not be interpreted as a new state-of-the-art on the standard BabyAI tasks.

4.2.2 HYPERPARAMETER SENSITIVITY

To evaluate WMG’s sensitivity to hyperparameter selection, we applied the tuned hyperparameter settings from Level 4 to new training runs on all other levels. Figure 6 shows moderate degradations in performance for all models. In particular, when the hyperparameter values tuned on Level 4 are used in Level 5 training runs, none of the models reach a 99% solution rate within 1 million training steps, but WMG with factored observations reaches higher levels of performance than the other models. Broadly, these results indicate that WMG is no more sensitive to hyperparameter settings than the baseline agents.

5 CONCLUSION AND FUTURE WORK

We designed the *Working Memory Graph* to investigate how Transformer-based models can improve the performance of RL agents. In order to effectively leverage factored observations, WMG applies

Level	1	2	3
WMG-factored	5.0	13.5	34.7
nr-WMG-factored	3.2	9.9	39.3
GRU-factored	8.0	42.6	313.9
WMG-flat	40.6	74.9	231.4
GRU-flat	36.9	55.3	188.9

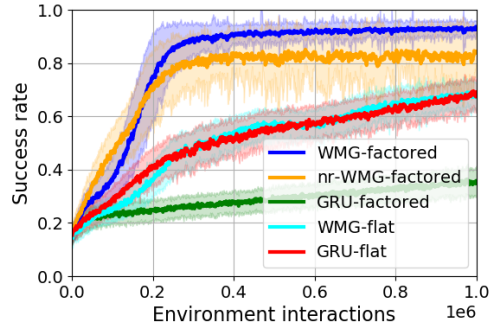


Figure 6: **Hyperparameter Sensitivity:** Sample efficiency (in thousands of environment interactions) of various model-format combinations using hyperparameters optimized for Level 4 then subsequently applied to Levels 1, 2, and 3 (left), as well as 5 (right). All model performances degrade, but WMG with factors still outperforms GRU-based models. Although none of the models reach the 99% threshold for Level 5, WMG reaches a high level of performance before the others. (See Table 1 for more details.)

Transformer-style self-attention to arbitrary numbers of percept vectors mapped directly to observed factors. And in order to represent multiple latent aspects of partially observable environments, without incurring large quadratic computational costs of self-attention over long histories, WMG incorporates a form of recurrence that creates shortcut paths of self-attention over a dynamic set of hidden states, called concepts.

We compared WMG’s performance to that of gated RNNs in two partially observable environments, one focused on complex reasoning over long-term dependencies, and one focused on reasoning over factored observations. In these experiments, WMG outperforms gated RNNs by wide margins. In particular, our results demonstrate that when factored observations are available, sample efficiency can be dramatically boosted by passing the factors separately to WMG percepts, instead of entangling the factors through concatenation into fixed-length vectors for processing by a gated RNN.

To clarify certain limitations of this version of WMG, we outline three potential enhancements:

Flexible concept lifetimes: In the work reported here, each new concept automatically replaces the oldest. A more flexible and adaptive concept-deletion scheme may improve WMG’s ability to model latent aspects in the environment. For instance, concept vectors that receive more attention than others may be the ones most worth keeping around for longer. Deleting a concept only when its recently-received attention falls below a certain threshold would allow the number of concept vectors to fluctuate somewhat over time, depending on the needs of the situation.

Graph edge content: As in the original Transformer, WMG applies input vectors to the nodes in its computation graph, but not to the edges between them. To better represent graph-structured data, Veličković et al. (2017) contemplated incorporating edge-specific data into Graph Attention Networks as future work. By harnessing the richer representational abilities of graph structures over set structures, a similar extension of WMG may allow it to better model complex relations among observed and latent factors in the environment.

Memory vectors: Various forms of external memory have been proposed in recent years. (Graves et al., 2016; Munkhdalai et al., 2019) Memory vectors retrieved from such stores could be fed to dedicated WMG *memory* nodes, in addition to the current concept and percept nodes, to further extend the range and flexibility of an agent’s effective time horizon.

ACKNOWLEDGMENTS

The authors wish to thank Alekh Agarwal and Xiaodong Liu for many valuable discussions.

REFERENCES

- Anonymous. Stabilizing transformers for reinforcement learning, 2019. URL <https://openreview.net/forum?id=SyxKrySYPr>. Under review, International Conference on Learning Representations, 2020.
- Dzmitry Bahdanau, Kyunghyun Cho, and Yoshua Bengio. Neural machine translation by jointly learning to align and translate, 2014. URL <http://arxiv.org/abs/1409.0473>. Accepted at ICLR 2015 as oral presentation.
- Craig Boutilier, Raymond Reiter, Mikhail Soutchanski, and Sebastian Thrun. Decision-theoretic, high-level agent programming in the situation calculus. In *Proceedings of the Seventeenth National Conference on Artificial Intelligence and Twelfth Conference on Innovative Applications of Artificial Intelligence*, pp. 355–362. AAAI Press, 2000. ISBN 0-262-51112-6. URL <http://dl.acm.org/citation.cfm?id=647288.721273>.
- Craig Boutilier, Ray Reiter, and Bob Price. Symbolic dynamic programming for first-order mdp. In *Proceedings of the 17th International Joint Conference on Artificial Intelligence - Volume 1, IJCAI'01*, pp. 690–697, San Francisco, CA, USA, 2001. Morgan Kaufmann Publishers Inc. ISBN 1-55860-812-5, 978-1-558-60812-2. URL <http://dl.acm.org/citation.cfm?id=1642090.1642184>.
- Maxime Chevalier-Boisvert, Dzmitry Bahdanau, Salem Lahlou, Lucas Willems, Chitwan Saharia, Thien Huu Nguyen, and Yoshua Bengio. Babyai: First steps towards grounded language learning with a human in the loop. *CoRR*, abs/1810.08272, 2018. URL <http://arxiv.org/abs/1810.08272>.
- Junyoung Chung, Kyle Kastner, Laurent Dinh, Kratarth Goel, Aaron Courville, and Yoshua Bengio. A recurrent latent variable model for sequential data. In *Proceedings of the 28th International Conference on Neural Information Processing Systems - Volume 2, NIPS'15*, pp. 2980–2988, Cambridge, MA, USA, 2015. MIT Press. URL <http://dl.acm.org/citation.cfm?id=2969442.2969572>.
- Jacob Devlin, Ming-Wei Chang, Kenton Lee, and Kristina Toutanova. BERT: pre-training of deep bidirectional transformers for language understanding. *CoRR*, abs/1810.04805, 2018. URL <http://arxiv.org/abs/1810.04805>.
- Anirudh Goyal, Alex Lamb, Jordan Hoffmann, Shagun Sodhani, Sergey Levine, Y. Bengio, and Bernhard Schölkopf. Recurrent independent mechanisms. *CoRR*, abs/1909.10893, 09 2019. URL <http://arxiv.org/abs/1909.10893>.
- Alex Graves, Greg Wayne, Malcolm Reynolds, Tim Harley, Ivo Danihelka, Agnieszka Grabska-Barwińska, Sergio Gómez Colmenarejo, Edward Grefenstette, Tiago Ramalho, John Agapiou, Adrià Puigdomènech Badia, Karl Moritz Hermann, Yori Zwols, Georg Ostrovski, Adam Cain, Helen King, Christopher Summerfield, Phil Blunsom, Koray Kavukcuoglu, and Demis Hassabis. Hybrid computing using a neural network with dynamic external memory. *Nature*, 538 (7626):471–476, October 2016. ISSN 00280836. URL <http://dx.doi.org/10.1038/nature20101>.
- Matthew J. Hausknecht and Peter Stone. Deep recurrent q-learning for partially observable mdp. *CoRR*, abs/1507.06527, 2015. URL <http://arxiv.org/abs/1507.06527>.
- Kaiming He, Xiangyu Zhang, Shaoqing Ren, and Jian Sun. Delving deep into rectifiers: Surpassing human-level performance on imagenet classification. *CoRR*, abs/1502.01852, 2015. URL <http://arxiv.org/abs/1502.01852>.
- Sepp Hochreiter and Jürgen Schmidhuber. Long short-term memory. *Neural Comput.*, 9(8):1735–1780, November 1997. ISSN 0899-7667. doi: 10.1162/neco.1997.9.8.1735. URL <http://dx.doi.org/10.1162/neco.1997.9.8.1735>.
- Leslie Pack Kaelbling, Michael L. Littman, and Anthony R. Cassandra. Planning and acting in partially observable stochastic domains. *Artif. Intell.*, 101(1-2):99–134, May 1998. ISSN 0004-3702. doi: 10.1016/S0004-3702(98)00023-X. URL [http://dx.doi.org/10.1016/S0004-3702\(98\)00023-X](http://dx.doi.org/10.1016/S0004-3702(98)00023-X).

-
- Diederik P. Kingma and Jimmy Ba. Adam: A method for stochastic optimization, 2014. URL <http://arxiv.org/abs/1412.6980>. 3rd International Conference for Learning Representations, San Diego, 2015.
- George A. Miller. The magical number seven, plus or minus two: Some limits on our capacity for processing information. *The Psychological Review*, 63(2):81–97, March 1956. URL <http://www.musanim.com/miller1956/>.
- Volodymyr Mnih, Koray Kavukcuoglu, David Silver, Andrei A. Rusu, Joel Veness, Marc G. Bellemare, Alex Graves, Martin Riedmiller, Andreas K. Fidjeland, Georg Ostrovski, Stig Petersen, Charles Beattie, Amir Sadik, Ioannis Antonoglou, Helen King, Dharshan Kumaran, Daan Wierstra, Shane Legg, and Demis Hassabis. Human-level control through deep reinforcement learning. *Nature*, 518(7540):529–533, February 2015. ISSN 00280836. URL <http://dx.doi.org/10.1038/nature14236>.
- Volodymyr Mnih, Adrià Puigdomènech Badia, Mehdi Mirza, Alex Graves, Timothy P. Lillicrap, Tim Harley, David Silver, and Koray Kavukcuoglu. Asynchronous methods for deep reinforcement learning. In *Proceedings of the 33rd International Conference on Machine Learning (ICML)*, pp. 1928–1937, 2016.
- Tsendsuren Munkhdalai, Alessandro Sordani, Tong Wang, and Adam Trischler. Metalearned neural memory. *CoRR*, abs/1907.09720, 2019. URL <http://arxiv.org/abs/1907.09720>.
- Junhyuk Oh, Valliappa Chockalingam, Satinder Singh, and Honglak Lee. Control of memory, active perception, and action in minecraft. In *Proceedings of the 33rd International Conference on Machine Learning - Volume 48, ICML'16*, pp. 2790–2799. JMLR.org, 2016. URL <http://dl.acm.org/citation.cfm?id=3045390.3045684>.
- Stuart Russell and Peter Norvig. *Artificial Intelligence: A Modern Approach*. Prentice Hall Press, Upper Saddle River, NJ, USA, 3rd edition, 2009. ISBN 0136042597, 9780136042594.
- Adam Santoro, Ryan Faulkner, David Raposo, Jack W. Rae, Mike Chrzanowski, Theophane Weber, Daan Wierstra, Oriol Vinyals, Razvan Pascanu, and Timothy P. Lillicrap. Relational recurrent neural networks. *CoRR*, abs/1806.01822, 2018. URL <http://arxiv.org/abs/1806.01822>.
- Ilya Sutskever, Oriol Vinyals, and Quoc V. Le. Sequence to sequence learning with neural networks. In *Proceedings of the 27th International Conference on Neural Information Processing Systems - Volume 2, NIPS'14*, pp. 3104–3112, Cambridge, MA, USA, 2014. MIT Press. URL <http://dl.acm.org/citation.cfm?id=2969033.2969173>.
- Ashish Vaswani, Noam Shazeer, Niki Parmar, Jakob Uszkoreit, Llion Jones, Aidan N. Gomez, Lukasz Kaiser, and Illia Polosukhin. Attention is all you need. *CoRR*, abs/1706.03762, 2017. URL <http://arxiv.org/abs/1706.03762>.
- Petar Veličković, Guillem Cucurull, Arantxa Casanova, Adriana Romero, Pietro Liò, and Yoshua Bengio. Graph attention networks. *CoRR*, abs/1710.10903, 2017. URL <http://arxiv.org/abs/1710.10903>.
- Oriol Vinyals, Igor Babuschkin, Wojciech M Czarnecki, Michaël Mathieu, Andrew Dudzik, Junyoung Chung, David H Choi, Richard Powell, Timo Ewalds, Petko Georgiev, et al. Grandmaster level in starcraft ii using multi-agent reinforcement learning. *Nature*, pp. 1–5, 2019.
- Vinicius Zambaldi, David Raposo, Adam Santoro, Victor Bapst, Yujia Li, Igor Babuschkin, Karl Tuyls, David Reichert, Timothy Lillicrap, Edward Lockhart, Murray Shanahan, Victoria Langston, Razvan Pascanu, Matthew Botvinick, Oriol Vinyals, and Peter Battaglia. Deep reinforcement learning with relational inductive biases, 2019.

Appendices

A PATHFINDING ENVIRONMENT DETAILS

A.1 GRAPH CONSTRUCTION ALGORITHM

The Pathfinding graph is constrained to be a polytree (singly-connected, directed acyclic graph) at each step of the episode, up to a maximum size of N patterns, each of size D , connected by $N - 1$ links. At the start of each episode, the graph contains a single random pattern. On each construction step, the environment links one new pattern to the graph through the following procedure (drawing all random numbers from uniform distributions):

1. Create a new random pattern $\mathbf{a}_i \in (-1, +1)^D$.
2. Randomly choose one existing pattern in the graph.
3. Create a new link, choosing a random direction, between the two patterns.

A.2 QUIZ-GENERATION ALGORITHM

On each quiz step, the environment first decides whether the correct answer should be 0 or 1 by sampling a binary value from a discrete uniform distribution. Then the environment draws uniform-random ordered pairs of nodes from the current graph until finding a pair that satisfies the desired answer. The observation is then constructed by concatenating the two pattern vectors and a value of 1 to mark this observation as a quiz.

A.3 *Depth-n* BASELINE ALGORITHM

The hand-coded baseline agent is configured with a depth parameter n . As new pattern pairs are revealed on graph-construction time steps, the agent maintains a growing vector of all patterns seen, and a growing matrix of directed path lengths from every observed pattern to every other. A path length of zero indicates that no path exists from the first pattern to the second. On each quiz step, the agent looks up from the matrix the path length len for the ordered pair of patterns in the observation. If $0 < len \leq n$, the agent chooses the *yes* action. Otherwise, the agent chooses the *no* action.

B TRAINING DETAILS AND HYPERPARAMETERS

Table 2: Fixed settings and options used for all experiments, except for the replicated baselines in Table 12.

Settings and options	Values
Dropout	None
Learning rate schedule	Constant learning rate
Non-linearities	ReLU, tanh
Parallel training workers	1
Optimizer	Adam (Kingma & Ba, 2014)
Parameter initialization, biases	0
Parameter initialization, non-bias weights	Kaiming uniform (He et al., 2015)
Reward shaping	None
Training algorithm	Advantage actor-critic (Mnih et al., 2016)
Weight decay regularization	None

Table 3: Tuned hyperparameter settings for Pathfinding experiments.

	WMG	nr-WMG	GRU
Actor-critic hidden layer size	128	128	512
Actor-critic t_{max}	16	16	16
Adam eps	1e-06	1e-08	1e-08
Discount factor γ	0.5	0.6	0.5
Entropy term strength β	0.01	0.005	0.02
Gradient clipping threshold	16.0	16.0	4.
GRU observation embedding size			256
GRU size			384
Learning rate	0.00016	0.00016	0.0001
Reward scale factor	2.0	1.0	0.5
WMG attention head size	12	16	
WMG attention heads	6	6	
WMG concept nodes	16	0	
WMG concept size	128		
WMG hidden layer size	12	32	
WMG layers	4	4	

Table 4: Tuned hyperparameter settings for BabyAI Level 1 - GoToObj.

	WMG factored	nr-WMG factored	GRU factored	WMG flat	GRU flat	CNN+GRU native 7x7x3
Actor-critic hidden layer size	2048	4096	4096	4096	2048	512
Actor-critic t_{max}	1	1	6	16	4	6
Adam eps	0.0001	1e-08	1e-08	1e-10	0.0001	1e-10
CNN hidden channel size 1						16
CNN hidden channel size 2						40
CNN hidden channel size 3						192
Discount factor γ	0.98	0.9	0.7	0.6	0.9	0.8
Entropy term strength β	0.002	0.05	0.01	0.005	0.02	0.02
Gradient clipping threshold	256.0	1024.0	512.0	512.0	128.0	128.0
GRU observation embed size			1024		512	512
GRU size			96		512	96
Learning rate	0.0001	4e-05	0.0004	0.0001	0.0001	0.0004
Reward scale factor	4.0	32.0	32.0	8.0	32.0	8.0
WMG attention head size	24	16		16		
WMG attention heads	4	10		12		
WMG concept nodes	1	0		1		
WMG concept size	64			256		
WMG hidden layer size	64	64		32		
WMG layers	4	4		1		

Table 5: Tuned hyperparameter settings for BabyAI Level 2 - GoToRedBallGrey.

	WMG factored	nr-WMG factored	GRU factored	WMG flat	GRU flat	CNN+GRU native 7x7x3
Actor-critic hidden layer size	4096	2048	4096	4096	4096	64
Actor-critic t_{max}	8	6	16	1	1	1
Adam eps	1e-06	1e-08	1e-10	1e-10	1e-06	0.0001
CNN hidden channel size 1						12
CNN hidden channel size 2						24
CNN hidden channel size 3						192
Discount factor γ	0.8	0.9	0.8	0.9	0.9	0.95
Entropy term strength β	0.01	0.02	0.01	0.005	0.005	0.02
Gradient clipping threshold	1024.0	512.0	1024.0	128.0	64.0	64.0
GRU observation embed size			4096		2048	256
GRU size			96		512	64
Learning rate	0.0001	0.00025	0.0001	2.5e-05	2.5e-05	0.0004
Reward scale factor	8.0	4.0	4.0	4.0	4.0	2.0
WMG attention head size	64	48		64		
WMG attention heads	4	1		3		
WMG concept nodes	1	0		8		
WMG concept size	32			64		
WMG hidden layer size	16	24		384		
WMG layers	3	3		1		

Table 6: Tuned hyperparameter settings for BabyAI Level 3 - GoToRedBall.

	WMG factored	nr-WMG factored	GRU factored	WMG flat	GRU flat	CNN+GRU native 7x7x3
Actor-critic hidden layer size	4096	2048	4096	4096	4096	4096
Actor-critic t_{max}	1	2	3	1	2	3
Adam eps	1e-12	0.0001	1e-06	0.0001	1e-06	0.01
CNN hidden channel size 1						12
CNN hidden channel size 2						40
CNN hidden channel size 3						192
Discount factor γ	0.95	0.9	0.9	0.9	0.9	0.9
Entropy term strength β	0.1	0.05	0.1	0.05	0.02	0.05
Gradient clipping threshold	128.0	128.0	128.0	128.0	32.0	32.0
GRU observation embed size			2048		4096	256
GRU size			192		512	64
Learning rate	2.5e-05	6.3e-05	6.3e-05	2.5e-05	2.5e-05	0.0004
Reward scale factor	8.0	4.0	8.0	8.0	4.0	4.0
WMG attention head size	128	32		24		
WMG attention heads	2	8		12		
WMG concept nodes	2	0		16		
WMG concept size	128			256		
WMG hidden layer size	64	32		128		
WMG layers	4	4		1		

Table 7: Tuned hyperparameter settings for BabyAI Level 4 - GoToLocal.

	WMG factored	nr-WMG factored	GRU factored	WMG flat	GRU flat
Actor-critic hidden layer size	2048	2048	1024	512	4096
Actor-critic t_{max}	6	3	3	6	4
Adam eps	1e-12	0.01	1e-06	1e-08	1e-12
Discount factor γ	0.5	0.6	0.95	0.5	0.9
Entropy term strength β	0.1	0.1	0.1	0.02	0.02
Gradient clipping threshold	512.0	512.0	256.0	256.0	512.0
GRU observation embed size			1024		512
GRU size			128		96
Learning rate	6.3e-05	0.0001	4e-05	2.5e-05	4e-05
Reward scale factor	32.0	16.0	8.0	16.0	2.0
WMG attention head size	128	64		24	
WMG attention heads	2	4		16	
WMG concept nodes	8	0		16	
WMG concept size	32			64	
WMG hidden layer size	32	48		16	
WMG layers	4	3		2	

Table 8: Tuned hyperparameter settings for BabyAI Level 5 - PickupLoc.

	WMG factored	nr-WMG factored
Actor-critic hidden layer size	512	2048
Actor-critic t_{max}	12	12
Adam eps	1e-10	1e-10
Discount factor γ	0.7	0.8
Entropy term strength β	0.02	0.05
Gradient clipping threshold	512.0	512.0
Learning rate	0.0001	6.3e-05
Reward scale factor	8.0	8.0
WMG attention head size	24	48
WMG attention heads	10	6
WMG concept nodes	8	0
WMG concept size	32	
WMG hidden layer size	128	96
WMG layers	2	2

C ADDITIONAL EXPERIMENTAL RESULTS

Table 9: Additional details for the Pathfinding experimental results in Figure 4 (right).

Models & algorithms	Final performance	Trainable parameters	Training speed
<i>Depth-(n-1)</i> baseline	100.0% of reward		
<i>Depth-3</i> baseline	99.7% of reward		
<i>Depth-2</i> baseline	97.6% of reward		
<i>Depth-1</i> baseline	86.9% of reward		
nr-WMG, full-history	99.6% of reward	204,963	96 steps/sec
WMG	99.6% of reward	132,507	91 steps/sec
GRU	94.7% of reward	1,139,459	291 steps/sec

Table 10: Number of trainable parameters, in thousands, for the BabyAI models in Table 1.

BabyAI level	WMG factored	nr-WMG factored	GRU factored	WMG flat	GRU flat	CNN+GRU native 7x7x3
1 - GoToObj	636	1,864	1,572	2,053	4,170	393
2 - GoToRedBallGrey	2,997	258	3,723	2,116	10,075	140
3 - GoToRedBall	3,418	2,217	3,749	3,229	15,126	709
4 - GoToLocal	2,235	1,960	1,137	2,022	1,479	—
5 - PickupLoc	879	2,007	—	—	—	—

Table 11: Training steps per second on a fixed machine, for the BabyAI models in Table 1.

BabyAI level	WMG factored	nr-WMG factored	GRU factored	WMG flat	GRU flat	CNN+GRU native 7x7x3
1 - GoToObj	38	28	146	111	86	149
2 - GoToRedBallGrey	58	113	147	35	18	88
3 - GoToRedBall	18	32	78	25	20	87
4 - GoToLocal	44	48	132	54	134	—
5 - PickupLoc	81	84	—	—	—	—

Table 12: BabyAI baseline agent sample efficiencies, defined as the amount of training (in either episodes or environment interaction steps) required for the agent to solve 99% of random episodes within 64 steps. The published results are the means of the min & max RL sample efficiencies reported in Table 3 of Chevalier-Boisvert et al. (2018). The replicated results are the medians over 10 training runs, using the code and default hyperparameter settings from the open source release of the BabyAI baseline agent. All numbers are in thousands.

BabyAI level	Instruction template	Published (<i>episodes</i>)	Replicated (<i>episodes</i>)	Replicated (interactions)
1 - GoToObj	GO TO color object	—	19	333
2 - GoToRedBallGrey	GO TO RED BALL	16	16	282
3 - GoToRedBall	GO TO RED BALL	272	283	3,674
4 - GoToLocal	GO TO color object	971	1,064	16,422
5 - PickupLoc	PICK UP color object loc	2,977	1,557	25,574